where η_m^* and τ_m^* represent the viscous parameter and relaxation time respectively at temperature T and they are given by Eqs. (32) and (33).

$$\eta_m^* = \eta_m \frac{dt}{dt_{T_0}} = \eta_m \exp\left(2.3026\beta\left(T - T_o\right)\right), \tag{32}$$

$$\tau_m^* = \tau_m \frac{dt}{dt_{T_0}} = \tau_m \exp\left(2.3026\beta\left(T - T_o\right)\right). \tag{33}$$

Eq. (32) shows the relation between the viscosity coefficient of the m^{th} Kuhn element at temperature T and its value at the reference temperature T_0. This is identical to the relationship obtained in Eq. (21). Similarly, Eq. (33) shows the relation between the relaxation time of the m^{th} Kuhn element at temperature T and its value at the reference temperature T_0 and this is identical to the relationship obtained in Eq. (22). Eqs. (30), (31), (32) and (33) constitute the internal variable formulation of the discrete generalized Kuhn model at any temperature T. The internal variable formulation is more general than the formulation based on the creep function, since it also holds in the multidimensional spaces of stress and strain tensors. Moreover, it does not depend on the existence of a closed form for the creep function and it can be used in cases of nonlinearities. It should be also mentioned that the internal variable formulation is amenable to a finite element implementation of the model.

RESULTS

The loss tangent given by Eq. (20) is used to fit the experimental results reported by Cerni (2001). Bitumen specimens are subjected to frequency sweep experiments at various temperatures and the plots of phase angle δ (in degrees) versus frequency (in Hz) at temperatures 6°C, 15°C and 25°C are obtained and shown in Fig. 5. Log scale has been used in the frequency axis. The parameters are estimated from model fit of the experimental results. The parameter estimation is done by nonlinear optimization techniques and programming is done in MATLAB. The objective function used for the parameter estimation is given by Eq. (34),

$$f = \sum_{i=0}^{M} \left(\frac{lt_{m,i} - lt_{expt,i}}{lt_{expt,i}} \right)^2, \tag{34}$$

where $lt_{m,i}$ and $lt_{expt,i}$ are i^{th} model and experimental loss tangent values and M is the total number of experimental data points. Fig. 5 shows the model fit at 6°C, 15°C, and 25°C. The values of the parameters are listed in Table 1. Fifteen Kuhn elements were used. It is noted that the values of the parameters A, α and r are temperature independent as they should.

This is a preview. Click here to purchase the full publication.

Table 1. List of parameters for various temperatures fit.

Temperature	A	B	C	α	r
$T_1=6^0C$	1.15	$B_1=25.10$	$C_1=0.0196$	0.43	1.01
$T_2=15^0C$	1.15	$B_2=34.30$	$C_2=0.0404$	0.43	1.01
$T_3=25^0C$	1.15	$B_3=48.52$	$C_3=0.0907$	0.43	1.01

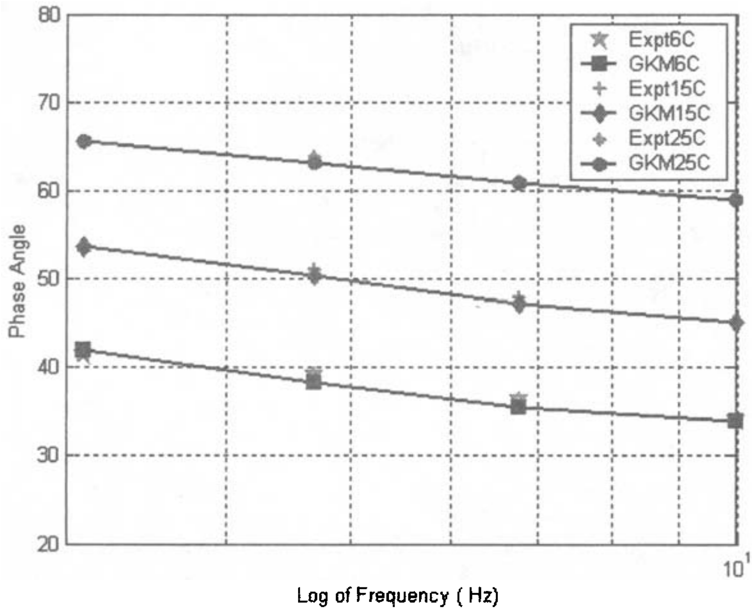

Figure 5. Loss tangent versus frequency; model fit to experimental data. The experimental data is from Cerni (2001).

For the validation of the model the following procedure is followed. Using the values of the parameters obtained for temperatures 6^0C and 15^0C, the values for the temperature dependent parameters B and C corresponding to 25°C are calculated. These calculated values are compared with the parameter values which have been obtained by the fitting process. For this, the slope β of the variation of the log of the shift factor a_T with temperature is calculated from Eq. (18) (treating T_1 as the reference temperature), i.e.

This is a preview. Click here to purchase the full publication.

$$C_2 = C_1 \exp\left(-2.3026\beta\left(T_2 - T_1\right)\right), \tag{35}$$

where T_1, T_2, C_1 and C_2 are given in Table 1. From Eq. (35), the value of the slope β is calculated as $\beta = -0.035$. Clearly, instead of Eq. (18), Eq. (19) could have been used.

The values of the parameters B and C for 25^0C are calculated from the following equations, using the obtained value for β.

$$C_3 = C_1 \exp\left(-2.3026\beta\left(T_3 - T_1\right)\right) = 0.0906, \tag{36}$$

$$B_3 = B_1 \exp\left(-2.3026\beta\left(T_3 - T_1\right)\alpha\right) = 48.49. \tag{37}$$

These calculated (predicted) values are almost equal to the fitted values B_3 and C_3 given in Table 1. This provides an excellent validation of the model, since the predicted values match the fitted ones. Therefore, the model is able to predict the variation of the loss tangent with the frequency of excitation at different temperatures by computing the corresponding to the temperatures parameters B and C, following the procedure just shown, and then using Eq. (20). We note that as is seen in Fig. 5, the loss tangent values are increasing with temperature, which means that the dissipated energy is higher at higher temperatures.

The model is validated against a second set of experiments reported by Corte (2001). In this case, dynamic shear tests were conducted at various temperatures on four different asphalt concrete mixes with penetration grades (PG) 10/20, 25/35, 35/50, and 50/70. Phase angle variation (in degrees) with temperature at 7.8 Hz has been recorded. In this case for each concrete mix Eq. (20) is expressed as a function of the temperature, and the parameters A, B, C, α, r, β, with the help of Eqs. (18) and (19). B and C are the values of the parameters at the reference temperature, taken here to be 0^0C. The objective function is given by Eq. (34). The parameters are tabulated in Table 2 and the number of Kuhn elements used for the fitting is 15. Fig. 6 shows the experimental results and the model's fit to the experimental data. It is evident from the figure that the generalized Kuhn model fits phase angle variation with respect to temperature with very good accuracy. The values of the parameters B_1 and C_1 at any other temperature can be obtained by using Eqs. (19) and (18) respectively and thus the phase angle value at this temperature is computed with the use of Eq. (20), for any of those four asphalt mixes and for frequency equal to 7.8 Hz.

This is a preview. Click here to purchase the full publication.

Table 2. List of parameters for phase angle versus temperature fit.

Parameters	PG 10/20	PG25/35	PG35/50	PG50/70
A	108.72	63.68	19.62	21.12
B	1722.3	8392.4	18431	6320.3
C	0.2099	0.0378	0.0057	0.008
α	0.3472	0.0511	0.0467	0.5388
r	1.05	1.05	1.05	1.05
β	-0.0149	-0.0196	-0.0196	-1.0302

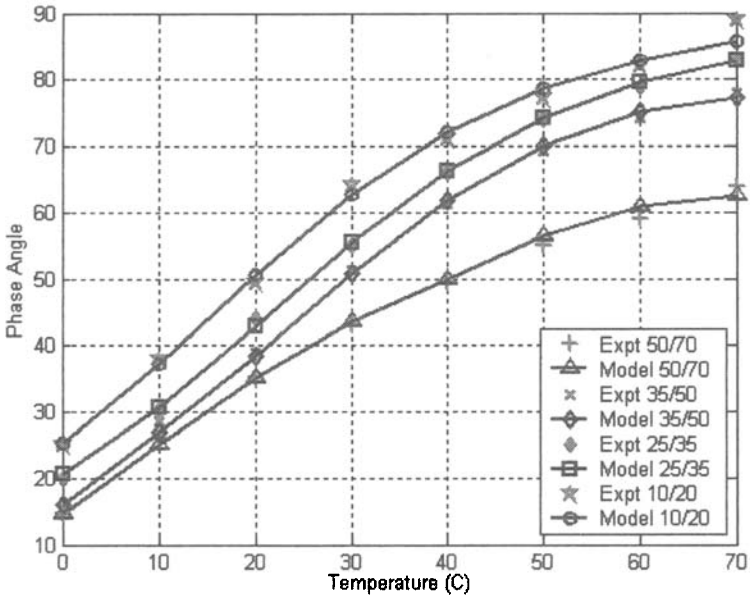

Figure 6. Model fit for phase angle versus temperature at 7.8 Hz. Experimental data is from Corte (2001).

Again, we observe from Fig. 6 that for all asphalt concrete mixes the phase angle (and hence the dissipated energy) increases with temperature, as it is expected.

This is a preview. Click here to purchase the full publication.

CONCLUSIONS

In this paper we developed a new temperature-dependent viscoelastic model for asphalt concrete. The new model has been presented in both a rheological form as well as in an internal variable one and has a small number of parameters. The creep function and the loss tangent of the model have been derived as functions of temperature. The model's comparisons to experimental data are very favorable. One of the contributions of this work is that a general methodology has been developed by which any viscoelastic model, which is expressed in terms of a creep function or in an internal variable form, can be made temperature-dependent. The advantages of the internal variable formulation have been discussed in the paper.

REFERENCES

Cerni, G. (2001). "Influence of the conditioning time on the rheological properties of bituminous at intermediate temperatures: Loading time-temperature-conditioning time superposition principle." *Road Materials and Pavement Design*, 2(4), 379- 401.

Corte, J. F. (2001). "Development and uses of hard-grade asphalt and of high-modulus asphalt mixes in France." *Transportation Research Circular*, Transportation Research Board, 503, 12-31.

FHWA. (1978). "Predictive design procedures". *VESYS Users Manual, Report No. FHWA-RD-77-154*, Federal Highway Administration.

Huang, Y. H. (1993). *Pavement analysis and design*, Prentice Hall, Englewood Cliffs, New Jersey.

Lubliner, J., and Panoskaltsis, V. P. (1992). "The modified Kuhn model of linear viscoelasticity." *International Journal of Solids and Structures*, 29 (24), 3099-3112.

Pagen, C. A.. (1965). "Rheological response of bituminous concrete." *Highway Research Record,* 67, Highway Research Board, 1-26.

Panoskaltsis, V. P., Papoulia, K. D., Bahuguna, S., and Korovajchuk, I. (2006). "The generalized Kuhn model of linear viscoelasticity." *In review*.

Panoskaltsis, V. P., Bahuguna, S., Papoulia, K. D., and Lubliner, J. (1999). "Finite element analysis of rate dependence and failure of concrete." *Proceedings of the European Conference on Computational Methods,* H.A. Mang et al. eds., 31 August - 3 September, 1999, Munich, Germany.

Williams, M. L., Landel, R. F., and Ferry, J. D. (1952). "Time temperature dependence of linear viscoelastic behavior." *Journal of Applied Physics*, 23, 838-843.

This is a preview. Click here to purchase the full publication.

LABORATORY VALIDATION OF VISCOELASTIC INTERCONVERSION FOR HOT MIX ASPHALT

Myung Goo Jeong[1], Amara Loulizi[2], P.E., and Gerardo W. Flintsch[3], M. ASCE

ABSTRACT: Various research efforts have proven that it is possible to interconvert the various linear viscoelastic material properties (i.e., the creep compliance, relaxation modulus, complex compliance, and dynamic modulus) of asphalt concrete materials. The interconversion makes it possible to predict one viscoelastic property from another and therefore eliminates the need to do more than one test to calculate all needed viscoelastic properties. This paper presents a laboratory validation of the interconversion between dynamic moduli and creep compliances obtained from two typical mixes used in the Commonwealth of Virginia. The measured dynamic modulus was successfully converted into creep compliance, and the measured creep compliance was successfully converted into dynamic modulus. Both converted properties were compared to the actual measured data. It was found that in most cases the converted properties were similar to the measured properties. However, the dynamic modulus predicted smaller creep compliance than was measured while the creep compliance predicted smaller dynamic modulus than was measured. This is attributed to the fact that the creep tests were performed at high, constant stress without confinement, which might have brought the material outside its linear viscoelastic range. More testing is therefore needed to confirm the promising results obtained with the existing conversion methods.

[1] Graduate Research Assistant (Former GRA at Virginia Tech, 2003~2005), Arizona State University, Department of Civil and Environmental Eng., PO Box 875306, Tempe, AZ 85287-5306, mgjeong@asu.edu

[2] Assistant Professor, Ecole Nationale d'ingénieur de Tunis, ENIT Département Génie Civil B.P. 37 Le Belvédère, 1002 Tunis, Tunisia, amlouliz@vt.edu

[3] Associate Professor, Charles Via, JR. Department of Civil and Environmental Engineering and , Director, Center for Sustainable Transportation Infrastructure, Virginia Tech Transportation Institute, 3500 Transportation Research Plaza, Blacksburg, VA 24061-0105, flintsch@vt.edu

This is a preview. Click here to purchase the full publication.

INTRODUCTION

Determining the viscoelastic properties of hot mix asphalt (HMA) is important for several applications, including modeling flexible pavement response to truck and environmental loadings, predicting the performance of the material in terms of specific distress types (e.g., low-temperature cracking and rutting), and for specifications as quality control measures (e.g., limiting a function of the dynamic modulus and the phase angle to a specified passing value).

Rheologists have studied the viscoelastic properties of polymers for many years, and the theory governing viscoelastic behavior of these materials is well established *(1)*. Among the tests used by rheologists to determine viscoelastic parameters are static creep compliance and dynamic modulus tests. These tests are now gaining wide acceptance among highway agencies to measure viscoelastic properties of HMA. Asphalt material researchers have proven that the interconversion between those viscoelastic properties measured on asphalt mixtures using the theory worker relatively well at low temperatures (i.e., linear condition) *(2)*.

In 2005, the Virginia Department of Transportation (VDOT) and the Virginia Tech Transportation Institute reviewed existing methods for determining the moduli of HMA and identified simple laboratory tests that accurately describe the constitutive behavior of HMA used in the Commonwealth of Virginia *(3)*. The performed tests evaluated included uniaxial static creep compliance and dynamic modulus. The results from that study presented an opportunity to verify whether existing interconversion methods between viscoelastic properties could be applied to the HMA at wider temperature ranges. This would eliminate the need to perform one of the two tests as the results from one test could be used to calculate the properties obtained from the other. This paper presents the measured data on both mixes, the procedure used to convert from one property to another and a comparison of the converted property with the measured data.

EXPERIMENTAL PROGRAM

Two typical HMA mixtures used in Virginia, SM-9.5A and BM-25.0, were used in this study. The SM-9.5A mix is a surface mix with a 12.5-mm maximum nominal aggregate size and a PG64-22 binder. The BM-25.0 is a base mix with a 25.0-mm maximum nominal aggregate size and a PG64-22 binder. The mixes were designed according to VDOT specifications *(4)*, which follow the SUPERPAVE procedures with some minor odifications. Table 1 shows the job mix formula with the source of the aggregates for both mixes. Table 2 presents the average aggregate gradation for both mixes.

All specimens prepared for testing were compacted using a Gyratory Compactor. The specimens were compacted to achieve approximately 4% ± 1% voids in total mix (VTM) for the molded specimen. Therefore, the specimens were compacted by fixing the height rather than fixing the number of required gyrations. Once a specimen was extracted from the TGC, its bulk density (G_{mb}) was measured using the AASHTO T166 procedure *(5)*, and then it was cored and cut to the final specimen

This is a preview. Click here to purchase the full publication.

dimensions of 102 mm by 152 mm. Another bulk density was then performed on the final specimen since it is known that there is a slight difference in the measured VTM between the compacted mold specimen and the final cored and cut specimen.

TABLE 1. Job mix formula for both mixes

Type (1)	Percentage (%) (2)	Source (3)	Location (4)
BM-25.0			
# 357 Limestone	18	ACCO STONE	Blacksburg, VA
#68 Limestone	30	ACCO STONE	Blacksburg, VA
#10 Limestone	27	ACCO STONE	Blacksburg, VA
Concrete Sand	10	WYTHE STONE	Wytheville, VA
Processed RAP	15	ADAMS Construction	Blacksburg, VA
PG 64-22	4.7	Associated Asphalt	Roanoke, VA
Adhere HP+	0.5	ARR-MAZ Products	Winter Haven, FL
SM-9.5A			
# 8 Quartzite	45	Salem Stone	Sylvatus, VA
#10 Quartzite	25	Salem Stone	Sylvatus, VA
Concrete Sand	15	Wythe Stone	Wytheville, VA
Processed RAP	15	ADAMS Construction	Blacksburg, VA
PG 64-22	5.5	Associated Asphalt	Roanoke, VA
Adhere HP+	0.5	ARR-MAZ Products	Winter Haven, FL

TABLE 2. Aggregate gradation for both mixes

Sieve Open. (mm) (1)	Sieve # (2)	% Passing (3)	
37.5	1.5	-	100.0
25	1	-	92.8
19	3/4	-	84.9
12.5	1/2	100.0	77.7
9.5	3/8	91.4	70.1
4.75	#4	56.3	48.4
2.36	#8	39.9	25.4
1.18	#16	31.2	17.4
0.6	#30	23.1	13.2
0.3	#50	14.2	8.0
0.15	#100	9.7	5.3
0.075	#200	7.4	4.3

Table 3 presents the G_{mb} and VTM values for all prepared specimens after extraction from the TGC and after coring and cutting. For the SM-9.5A mix, the average VTM for the dynamic modulus specimens were 4.2% and 2.7% right after extraction from the TGC and after coring and cutting, respectively. The static creep test specimens had 4.3% and 3.1% VTM after extraction from the TGC and after

This is a preview. Click here to purchase the full publication.

coring and cutting, respectively. For the BM-25.0 mix, on average, the VTM for the dynamic modulus specimens were 5.0% and 3.7% right after extraction from the TGC and after coring and cutting, respectively. The static creep test specimens had 5.0% and 3.6% VTM after extraction from the TGC and after coring and cutting, respectively.

TABLE 3. G_{mb} and VTM for all prepared specimens

	Dynamic Modulus					Static Creep				
		Extracted Specimen		Final Specimen			Extracted Specimen		Final Specimen	
	Label (1)	G_{mb} (2)	VTM (%) (3)	G_{mb} (4)	VTM (%) (5)	Label (6)	G_{mb} (7)	VTM (%) (8)	G_{mb} (9)	VTM (%) (10)
SM-9.5A	S93	2.365	4.1	2.402	2.6	S109	2.363	4.2	2.400	2.7
	S94	2.366	4.1	2.402	2.6	S110	2.364	4.2	2.405	2.5
	S95	2.365	4.1	2.398	2.8	S111	2.361	4.3	2.396	2.9
	S96	2.367	4.1	2.403	2.6	S112	2.358	4.4	2.393	3.0
	S97	2.368	4.0	2.427	1.6	S113	2.370	3.9	2.406	2.5
	S98	2.363	4.2	2.392	3.0	S114	2.365	4.1	2.395	2.9
	S101	2.364	4.2	2.399	2.7	S115	2.356	4.5	2.392	3.1
	S102	2.360	4.3	2.388	3.2	S116	2.362	4.3	2.387	3.2
	S105	2.366	4.1	2.392	3.1	S117	2.356	4.5	2.362	4.2
	S107	2.362	4.3	2.388	3.2	S119	2.362	4.3	2.368	4.0
	Average	**2.365**	**4.2**	**2.399**	**2.7**	**Average**	**2.362**	**4.3**	**2.390**	**3.1**
BM-25.0	B56	2.473	4.9	2.510	3.5	B55	2.464	5.2	2.510	3.5
	B62	2.473	4.9	2.511	3.4	B58	2.467	5.1	2.509	3.5
	B63	2.470	5.0	2.517	3.2	B60	2.463	5.3	2.493	4.2
	B64	2.473	4.9	2.496	4.0	B61	2.474	4.9	2.499	3.9
	B65	2.465	5.2	2.511	3.5	B78	2.478	4.7	2.517	3.2
	B67	2.473	4.9	2.497	4.0	B79	2.471	5.0	2.518	3.2
	B68	2.471	5.0	2.502	3.8	B80	2.462	5.3	2.498	4.0
	B69	2.471	5.0	2.508	3.6	B81	2.466	5.2	2.514	3.3
	B76	2.470	5.0	2.488	4.3	B84	2.470	5.0	2.500	3.9
	B77	2.474	4.9	2.513	3.4	B85	2.476	4.8	2.509	3.5
	Average	**2.471**	**5.0**	**2.505**	**3.7**	**Average**	**2.469**	**5.0**	**2.507**	**3.6**

The dynamic modulus and static creep tests were performed with the same servo-hydraulic machine and using the same extensometers to measure the vertical deformations. Five temperatures were used: -15°C, 5°C, 20°C, 30°C, and 40°C. For the static creep test, the applied load was sustained for 1,000 seconds, while for the dynamic modulus test, six frequencies were used: 0.1 Hz, 0.5 Hz, 1 Hz, 5 Hz, 10 Hz, and 25 Hz. In both tests, two specimens were tested per temperature; therefore, 10 specimens per mix and per test were tested in total, as is presented in Table 3.

DYNAMIC MODULUS

Table 4 presents the average measured dynamic modulus and the phase angle for both mixes. As expected, under a constant loading frequency, the magnitude of the

This is a preview. Click here to purchase the full publication.

dynamic modulus decreases with an increase in temperature; and under a constant testing temperature, the magnitude of the dynamic modulus increases with an increase in frequency. On the other hand, the phase angle decreases as the frequency increases at testing temperatures of -15°C, 5°C, and 20°C. However, at testing temperatures of 30°C and 40°C, the behavior of the phase angle as a function of frequency is more complex, which is attributed to the aggregate interlock that controls the response of the specimen at high temperatures and low frequencies as reported by other researchers *(6)*.

The average measured data were used to construct a master curve for the dynamic modulus at a reference temperature of 20°C. The method developed by Pellinen and Witczak was used in this study to construct the master curve *(7)*. The method consists of fitting a sigmoidal curve to the measured dynamic modulus test data using nonlinear least-square regression techniques. The shift factors at each temperature are determined simultaneously with the other coefficients of the sigmoidal function. The calculated shift factors for the SM-9.5A mix and the BM-25.0 mix are shown in Figures 1a and 1b, respectively. The best-fit sigmoidal functions for the SM-9.5 mix and BM-25.0 mix are given by Equations 1 and 2, respectively.

$$\log\left|E^*\right| = 1.8762 + \frac{2.41534}{1+e^{-1.28301-0.59499\log f_r}} \tag{1}$$

$$\log\left|E^*\right| = 2.1358 + \frac{2.26117}{1+e^{-1.11630-0.62793\log f_r}} \tag{2}$$

TABLE 4. Average dynamic modulus (MPa) and phase angle (°) results

	-15°C		5°C		20°C		30°C		40°C	
	|E*| (1)	δ (2)	|E*| (3)	δ (4)	|E*| (5)	δ (6)	|E*| (7)	δ (8)	|E*| (9)	δ (10)
SM-9.5A Frequency (Hz)										
25	19,563	1.2	13,833	6.0	11,312	15.1	6,722	24.3	3,484	32.1
10	19,117	2.4	12,058	7.9	9,787	17.3	5,432	25.2	2,521	29.8
5	18,750	3.0	11,313	8.7	8,609	19.2	4,384	27.1	1,985	28.6
1	18,285	3.4	10,118	10.9	5,953	24.2	2,635	28.8	1,226	23.9
0.5	17,528	3.7	8,804	12.8	4,734	29.8	2,054	31.5	709	28.3
0.1	15,940	5.1	7,432	16.3	2,890	33.4	1,316	28.2	532	19.6
BM-25.0 Frequency (Hz)										
25	24,483	1.3	18,687	8.0	13,395	15.1	7,978	23.1	4,029	30.7
10	24,243	2.8	17,431	7.8	11,549	17.1	6,568	24.4	3,122	28.5
5	23,867	3.0	16,485	9.1	10,104	19.1	5,366	26.1	2,843	26.5
1	22,484	3.9	13,993	11.1	6,952	23.9	3,246	29.5	1,708	23.0
0.5	21,428	4.7	12,426	13.5	5,534	29.2	2,132	36.9	956	27.8
0.1	19,991	5.8	10,408	16.6	3,419	33.6	1,316	35.1	725	20.5

This is a preview. Click here to purchase the full publication.